

Simulated tropical cyclonic winds for low cycle fatigue loading of steel roofing

David J. Henderson* and John D. Ginger

Cyclone Testing Station, James Cook University, Townsville, Queensland, Australia

Murray J. Morrison and Gregory A. Kopp

Boundary Layer Wind Tunnel Laboratory, University of Western Ontario, London, Ontario, Canada

(Received February 16, 2009, Accepted May 7, 2009)

Abstract. Low rise building roofs can be subjected to large fluctuating pressures during a tropical cyclone resulting in fatigue failure of cladding. Following the damage to housing in Tropical Cyclone Tracy in Darwin, Australia, the Darwin Area Building Manual (DABM) cyclic loading test criteria, that loaded the cladding for 10000 cycles oscillating from zero to a permissible stress design pressure, and the Experimental Building Station TR440 test of 10200 load cycles which increased in steps to the permissible stress design pressure, were developed for assessing building elements susceptible to low cycle fatigue failure. Recently the ‘Low-High-Low’ (L-H-L) cyclic test for metal roofing was introduced into the Building Code of Australia (2007). Following advances in wind tunnel data acquisition and full-scale wind loading simulators, this paper presents a comparison of wind-induced cladding damage, from a “design” cyclone proposed by Jancauskas, *et al.* (1994), with current test criteria developed by Mahendran (1995). Wind tunnel data were used to generate the external and net pressure time histories on the roof of a low-rise building during the passage of the “design” cyclone. The peak pressures generated at the windward roof corner for a tributary area representative of a cladding fastener are underestimated by the Australian/New Zealand Wind Actions Standard. The “design” cyclone, with increasing and decreasing wind speeds combined with changes in wind direction, generated increasing then decreasing pressures in a manner similar to that specified in the L-H-L test. However, the L-H-L test underestimated the magnitude and number of large load cycles, but overestimated the number of cycles in the mid ranges. Cladding elements subjected to the L-H-L test showed greater fatigue damage than when experiencing a five hour “design” cyclone containing higher peak pressures. It is evident that the increased fatigue damage was due to the L-H-L test having a large number of load cycles cycling from zero load ($R=0$) in contrast to that produced during the cyclone.

Keywords: wind loads; design; pressure; tropical cyclone; damage; cladding; fatigue; test.

1. Introduction

The roofs of low-rise buildings are subjected to large pressures during windstorms. The creation of a dominant opening in the windward wall by debris impact, door failure, etc, can generate large

* Corresponding Author, E-mail: David.Henderson@jcu.edu.au

positive internal pressures, which, in combination with large suctions at the edges of the roof, will generate large net pressures (Ginger and Henderson 2003). This scenario is commonly responsible for much of the damage to buildings, and is usually the design criterion in cyclone regions.

Tropical Cyclone 'Tracy' caused catastrophic damage to housing in Darwin in 1974; Walker (1975) reported over 90% of houses and 70% of other structures suffered significant loss of roof cladding. These losses were caused by low cycle fatigue of the cladding adjacent to its fasteners, as shown in Fig. 1(a) (Morgan and Beck 1977). Following the impact of Cyclone 'Larry' on Innisfail in 2006, fatigue failure of pierced fixed metal cladding, shown in Figure 1(b), was observed in a few instances even though the cyclone's peak winds were less than the required design values for the region, as the distance between fixing centres greatly exceeded typical product specifications (Ginger, *et al.* 2007).

Metal roof cladding used in cyclonic regions of Australia are required to be evaluated by the recently introduced Low-High-Low (L-H-L) test, specified in the Building Code of Australia (Australian Building Codes Board 2007), to ultimate limit state design wind loads. This test was introduced with the premise of unifying the test criteria for the cyclonic regions of Australia and superseding the previous TR440 (Experimental Building Station 1978) and DABM (Darwin Reconstruction Commission 1976) tests (described in Henderson, *et al.* 2001), which were introduced following the devastation caused by Cyclone 'Tracy'. The definition of failure for a test is the disengagement of the cladding from fixings. The failure typically results from cracking at the fixing or connection failures. Revisions to these tests were based on extensive research and testing by Mahendran (1995) using external pressures measured on a building model in a wind tunnel experiment by Jancauskas, *et al.* (1994). However, these studies did not incorporate the effects of internal pressure resulting from dominant openings in the building envelope.

The wind load acting on a part of the roof of a building during a cyclone event will depend on the parameters of the cyclone such as the peak and mean wind speeds, size and translational speed of the cyclone, as well as building geometry and internal pressures. Buildings located in the path of a cyclone near the radius of maximum winds just outside the eye of the cyclone (where the highest wind speeds are usually found), are generally subjected to the largest wind loads. The variation of external pressure (i.e. magnitude and cycles) will depend on the characteristics of the cyclone,

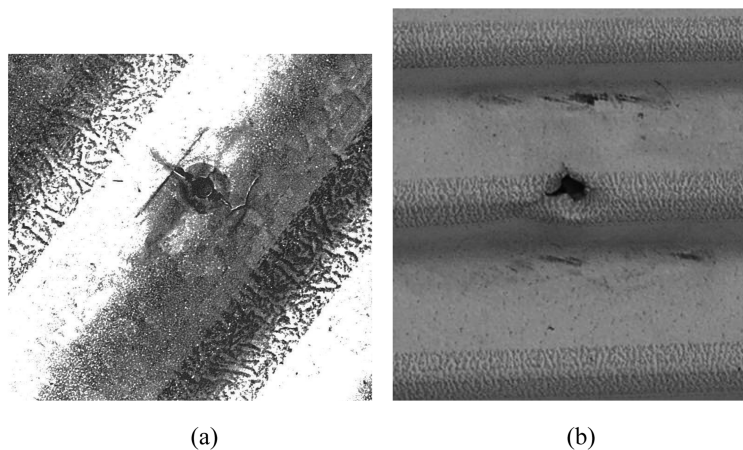


Fig. 1 Cracking patterns following (a) Cyclone 'Tracy' and (b) Cyclone 'Larry'

building shape, and orientation with respect to the passage of the cyclone. For instance, a cyclone travelling slowly is expected to generate a larger number of pressure cycles of the same intensity than a cyclone with the same intensity but moving faster, whilst an increase in the wind speed is expected to increase the pressure as well as the number of cycles in a given time span.

This paper analyses the variation of pressure near the windward edge of a gable roof building with and without a dominant opening, during the passage of a “design” cyclone detailed by Jancauskas, *et al.* (1994). The pressures were compared with design pressures derived from AS/NZS1170.2:2002 (Standards Australia 2002). Following this, the pressure fluctuations on this part of the roof were quantified in terms of the number of pressure cycles (mean, peak and range) and compared with current L-H-L test specifications. The analysis was carried out using pressures measured on a 1/100 model-scale building at the University of Western Ontario (UWO). Finally, a specimen of roof cladding was subjected to a dynamic wind load simulating the “design” cyclone, and its performance assessed.

2. The “design” tropical cyclone

Wind loading codes and standards such as AS/NZS1170.2:2002 (Standards Australia 2002) specify ultimate limit state design wind speeds based on return periods of 500 to 1000 yrs for design of normal buildings. In cyclonic Region C of Australia, this design gust wind speed (V_{500}) is 69.3 m/s at a 10m elevation in open country terrain (Terrain Category 2 according to AS/NZS1170.2:2002). The wind field (speed and direction) in a region impacted by a cyclone is dependent on the characteristics of the cyclone, the approach terrain and topography and the location with respect to the passage of the cyclone. The variation of wind speed and direction measured in cyclones indicate an increasing wind speed as the cyclone approaches, followed by a drop in the wind speed combined with a change in wind direction as it travels past the measurement point.

The wind load acting on a part of a structure can be analysed by combining time varying pressure coefficients with the corresponding approach wind speed and direction. Although the overall change in direction could be 180°, it is assumed that the change in direction during the critical, intense period of the cyclone is about 90°, as assumed by Jancauskas, *et al.* (1994) in their “design” cyclone. Jancauskas, *et al.* (1994) used a 3 s peak to mean gust factor of approximately 1.7 in analysing the wind speeds. Recent measurements and analysis, have shown that the gust factor can be in the order of 1.4 to 1.7 for coastal open terrain depending on factors such as roughness, on-shore or off-shore winds, etc (Harper, *et al.* 2008). A lower gust factor will give a higher mean wind speed for the same gust wind speed.

To enable a comparison of results, the roof loads are determined for a mid-range category 4 cyclone (with a peak 3 s gust wind speed of 70 m/s) with the variation of 10 min mean wind speed and direction shown in Figure 2, taken from Jancauskas, *et al.* (1994), which they based on the analysis of parameters from destructive cyclones such as Cyclone ‘Tracy’ and Cyclone ‘Winifred’ (Innisfail, Queensland 1986). Mahendran (1995) used this “design” cyclone to develop the L-H-L test. The cyclone has a radius to maximum winds of 25 km and a translational speed of 15 kph. The duration of a cyclone (i.e. slow or fast translational speed) will greatly affect the potential for wind induced fatigue damage (Ginger, *et al.*, 2007). The variation of pressure on the roof is analysed for wind speeds and directions derived from this “design” cyclone.

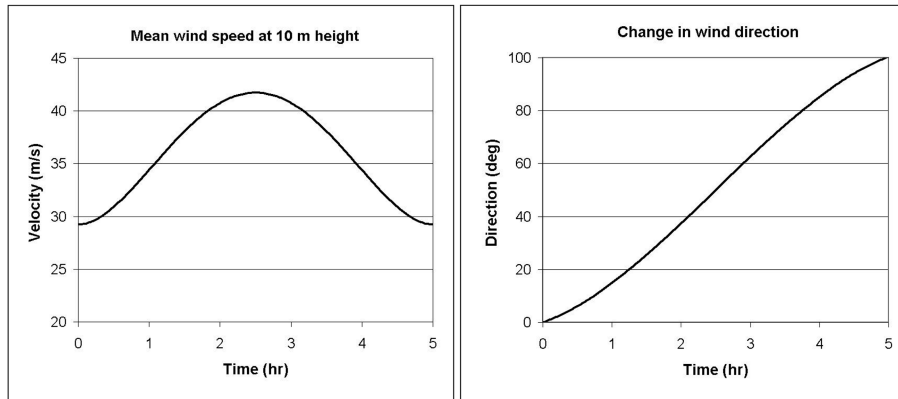


Fig. 2 Variation of mean wind speed and direction over time (Jancauskas, *et al.* 1994)

3. Building configurations

A range of generic low-rise building models were tested in the wind tunnel at the University of Western Ontario (UWO) in Canada, as part of a project initiated by the National Institute of Standards and Technology (NIST) of the United States. The project provides a validated, quality controlled set of model scale measurements for use in analysing wind loads on buildings. For complete details of the test set-up and model configurations, refer to Ho, *et al.* (2005). Detailed comparisons with previously published data and with current building codes or standards (including AS/ NZS1170.2:2002 (Standards Australia 2002) can be found in St. Pierre, *et al.* (2005), while analysis of internal pressures can be found in Oh, *et al.* (2007). Pressure measurements from this database are used for the analysis conducted in this paper.

3.1. The NIST model building

The data used herein was obtained for a model building with equivalent full-scale plan dimensions of 38.1 m × 24.4 m, a gable end roof of slope 1:12 and an eaves height of 4.88 m in the Boundary Layer Wind Tunnel II at UWO. This building configuration, shown in Fig. 3, was tested at a length scale of 1/100 in a simulated open approach atmospheric boundary layer. The mean wind speed at the reference height of 10 m was 8.8 m/s so that $Re = 30,000$ based on the eave height. External point pressures measured at points R1 and R2 on the roof and W1 on the wall, as shown in Fig. 3, for approach winds over a 180° range in 5° intervals, are used in this paper. A 762 mm long, tuned, tubing system connects each tap to high speed pressure scanners as described by Ho, *et al.* (2005). Fluctuating pressures at these taps which were essentially measured simultaneously were sampled at 500 Hz for 100 s, for a single run. Measured mean and peak pressures are defined in terms of a pressure coefficient, $C_p = p / (\frac{1}{2}\rho\bar{U}^2)$; where, p is the pressure and $\frac{1}{2}\rho\bar{U}^2$ is the mean dynamic pressure at mid-roof height.

Pressure acting towards the surface is defined as positive. A full-scale mean wind speed of 42 m/s, at the reference height of 10 m, gives a velocity scale of $U_r = 1/4.7$. Combined with the length scale $L_r = 1/100$, gives a time scale $T_r = 0.047$, essentially meaning that the 100 s in model scale is equivalent to 35 minutes, in full-scale, sampled at 24 Hz. However, as the analysis is carried out for

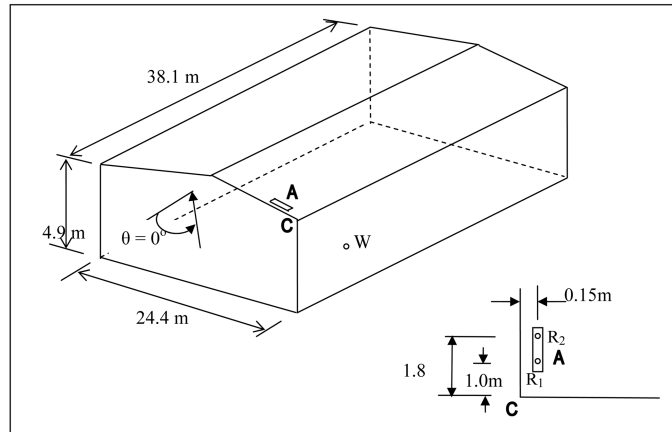


Fig. 3 Full scale dimensions and pressure tap locations on the NIST building also showing roof corner region C (not to scale)

15 minute blocks in full scale, the corresponding number of samples in model scale needs to be determined. In the case where the full-scale mean wind speed varies according to Fig. 2, the relationship between the time span in the wind tunnel and full-scale and the relevant cycles in model and full-scale is given by Eq. (1).

$$N_f = N_m \cdot (L_r / U_r) \cdot (T_f / T_m) \tag{1}$$

Here

- N_f – Number of cycles in full scale
- N_m – Number of cycles in model scale
- T_m – Time in model scale (i.e., 100 seconds)
- T_f – Time in full scale (i.e., 15 minutes)

Pressures measured at individual taps are combined to give area averaged pressure acting on the taps R1 and R2, representative of the load on the 0.16 m × 0.9 m cladding fastener tributary area, A, shown in Fig. 3.

3.2. AS/NZS 1170.2 wind loads

Wind loads for the design of cladding and fixings on low-rise buildings are usually calculated from pressures derived using nominal shape factors or pressure coefficients, provided in AS/NZS 1170.2:2002 (Standards Australia 2002). The peak (i.e. design) external pressures are calculated from Eq. (2), where ρ is the density of air, and C_{fig} is the aerodynamic shape factor. For external and internal pressures, the aerodynamic shape factors are $C_{fig} = C_{p,e}(K_a \times K_c \times K_l \times K_p)$ and $C_{fig} = C_{p,i} \times K_c$, respectively. The relevant external and internal pressure coefficients, $C_{p,e}$, and $C_{p,i}$, are obtained from Section 5, and Appendix C in AS/NZS 1170.2:2002, and K_a , K_c , K_l and K_p are factors for area-averaging, load combination, local-pressure effects, and cladding permeability. The dynamic response factor C_{dyn} is taken equal as 1.0 for these types of (i.e. “static”) structures, and $V_{des,\theta}$ is the 3sec peak design gust wind speed at mid-roof height.

$$\hat{p}, \tilde{p} = 0.5 \rho V_{des, \theta}^2 C_{fig} C_{dyn} \quad (2)$$

AS/NZS1170.2:2002 (Standards Australia 2002) gives an external pressure coefficient $C_{p,e}$ of -0.9 for area A for the wind directions of interest in this study, and internal pressure coefficients $C_{p,i}$ of 0 and 0.7 for the nominally sealed and dominant windward wall opening cases. A local pressure factor K_l of 2.0 applies for the design of cladding and fixings, located in an area $< a^2/4$ and within a distance $a/2$ from the windward roof edge, and a K_l of 1.5 applies in an area $< a^2$ and within a distance a from the windward roof edge. Here ‘ a ’ is the minimum of $0.2d$, $0.2b$ or h . Accordingly, $a = 4.88$ m, and K_l of 2.0 applies to the cladding fastener area A. The area reduction factor K_a , the combination factor K_c , and the porosity factor K_p all equal 1.0.

For the specified building geometry in Fig. 3, situated in open terrain, AS/NZS 1170.2:2002 specifies external design pressures of -4.78 kPa with a K_l of 2.0 on the roof, and 1.86 kPa on the wall, for a regional ultimate limit states (ULS) design wind speed of 69.3 m/s.

4. Wind loads

Area averaged peak (minimum and maximum) external pressure coefficients acting on taps R1 and R2 representative of the cladding fastener area, A , and the wall, W , for wind directions $\theta = 0^\circ$ to 180° are shown in Fig. 4. The large suction pressures are generated on area A (taps adjacent to the gable end) by the formation of conical vortices for $\theta = 30^\circ$ to 60° . Positive pressures greater than 2 kPa are experienced on the wall area W , for $\theta = 45^\circ$ to 110° .

The variation of peak external suctions on roof area A and peak external positive pressures on wall area, W , with the passage of the “design” cyclone, for two building orientations (labelled as I and II), are shown in Figs. 5(a) and 5(b). Orientation I was derived by taking the wind direction for which the largest mean C_p occurred for area A , while orientation II was chosen when the mean wall pressure was positive for the complete passage of the “design” cyclone. The building orientations shown in each figure are for 2.5 hours into the “cyclone”, that is, when the 42 m/s mean wind speed corresponds to the direction shown. Fig. 5(a) shows the peak pressures for areas A and W are -6.6 and 2.2 kPa for building orientation I, while Fig. 5(b) shows the peaks are -4.6 and 2.8 kPa for building

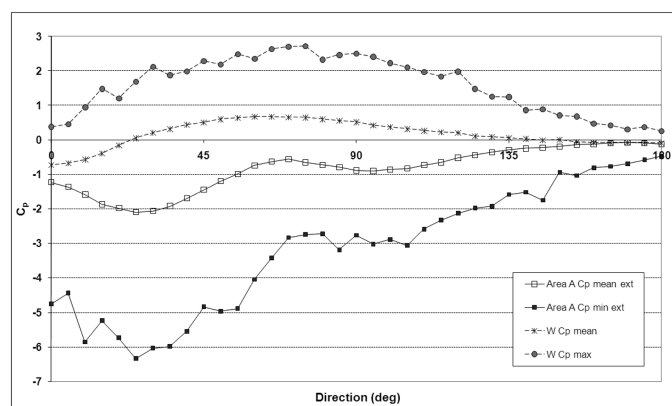


Fig. 4 Peak and mean pressure coefficients on areas A and W as a function of wind angle

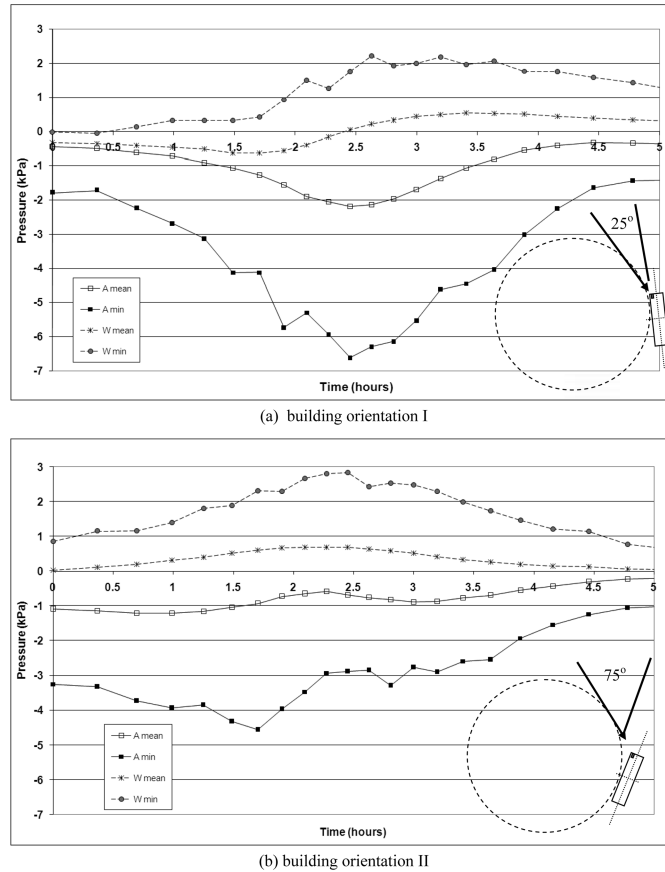


Fig. 5 Peak and mean pressures

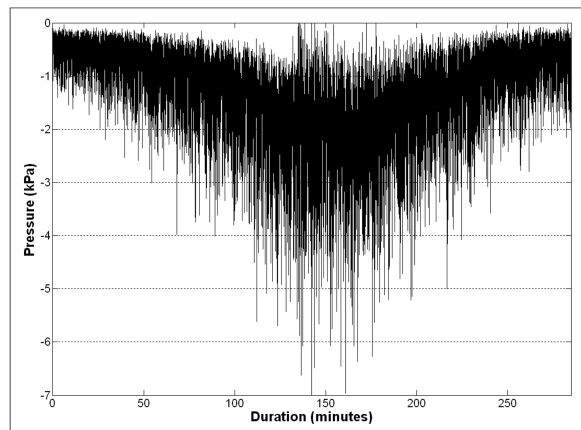
orientation II.

Since the analysis is based on the wind tunnel time series data, it should be noted that the presented peaks are from the portion of data record used and are not the peaks derived from an extreme value analysis that would form the basis for a quasi-static structural design. Even though the data does not include the extreme peaks, from the design pressures calculated in Section 3.2, it can be seen that AS/NZS 1170.2:2002 (Standards Australia 2002) underestimates the design pressures on cladding fasteners (area *A*). This is in keeping with findings by Ginger and Henderson (2003) who analysed the characteristics of the external, and the combined external and internal (i.e., net) pressures on the full-scale Texas Tech building, and showed that significantly higher pressures than those specified in standards such as AS/NZS 1170.2:2002 could be experienced near the windward roof edge. This shortcoming would be partly redressed by a proposed amendment to AS/NZS1170.2:2002 with an increase in K_f for small tributary areas at the corners of roofs.

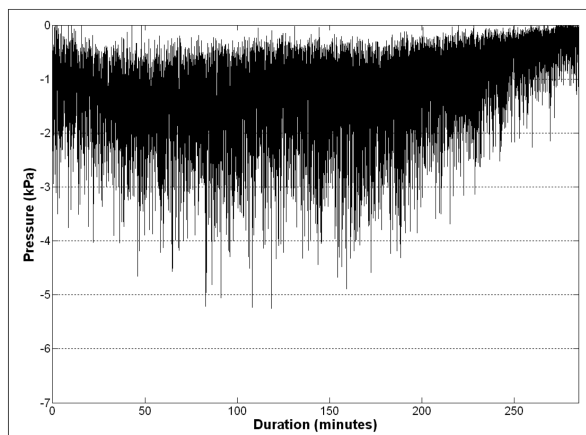
Although the internal pressure will be small in the case of the building remaining nominally sealed, a dominant opening can significantly increase the internal pressure and also the net pressure for certain approach wind directions (Oh, *et al.* 2007, Kopp, *et al.* 2008). For building orientation I, the net pressures across roof area *A* are calculated for a scenario assuming that a dominant opening will most likely be created on the long wall, near the position of the wall tap, *W*, at the peak of the

cyclone. This is analogous to a windward window breaking or a door blowing inwards at approximately the 2.5 hour mark. For building orientation II, it is assumed that the W dominant opening is present for the total duration of the cyclone. The internal pressures are taken to be equal to the external pressure fluctuations at the opening. This is a reasonable assumption based on the analysis by Ginger, *et al.* (2008) who showed that the internal pressure fluctuations will range between about 0.8 to 1.2 times the external pressure at a dominant opening for most combinations of opening size, building volume and approach wind speed.

The variation of the net pressures on roof area A for both building orientations for the change in wind direction with the change in wind speed is shown in Figs. 6(a) and 6(b). The peak net pressures for building orientations I and II are -7.1 and -5.2 kPa, respectively. Fig. 6(a) clearly shows the increasing and then decreasing wind loads on area A , in a form similar to that specified by L-H-L test. Fig. 6(b) has the increasing and decreasing pressures but not as pronounced as building orientation I, due to its lower external peak and the application of positive internal pressures for the whole duration. Both figures highlight the fluctuating nature of the roof pressures having varying means, peaks, ranges and load ratios, R , defined in Section 5.



(a) building orientation I



(b) building orientation II

Fig. 6 Net pressures for varying wind angle and mean wind speed over time

5. Fatigue of cladding systems

Fatigue failure occurs when a component fails following the application of a series of fluctuating loads of lower magnitude than the component’s static strength. Common engineering components are manufactured in many different shapes and are connected with bolts, screws, or welds, etc. These changes in geometry, or holes for fixings, or flaws and stresses in welds, can create stress concentrations (i.e. magnify the nominal stresses resulting from applied loads), which are often responsible for rapid crack growth. During fluctuating loads, the crack grows as its tip extends into an area of plastic deformation. If crack growth continues (not necessarily at higher loads) the reduction in cross section can result in a sudden failure.

5.1. Load cycles

A single loading cycle acting on a structural component can be represented as shown in Fig. 7, where the load varies between a maximum, S_{max} and a minimum S_{min} , with a mean value $S_{mean} = (S_{max} + S_{min})/2$, a range $\Delta S = |S_{max} - S_{min}|$ and an amplitude $S = \Delta S/2$. Furthermore, a load ratio is defined as $R = S_{min}/S_{max}$, giving $R = -1$ for alternating loads (i.e., $S_{max} = -S_{min}$ or in other words $S_{mean} = 0$). For pulsating loads $R = 0$ (e.g. $S_{min} = 0$ or, in other words, $S_{mean} = S$).

5.2. Cladding behaviour

The fatigue behaviour of cladding is dependent on the load causing local plastic deformation (LPD), seen as dimpling under the screws around the fastener holes. This is around 600 N per fastener, for G550 (550 MPa minimum yield strength) 0.42 mm corrugated cladding fixed without cyclone washers. This LPD strength strongly influences the fatigue life. The resistance to fatigue of the corrugated cladding increases markedly if the cyclic load per fastener is kept below this LPD load (Beck and Stevens 1979, Mahendran 1990, Xu 1993). Beck and Stevens (1979) defined this cladding fatigue failure as low cycle fatigue because failure was typically within 10000 load cycles. Conversely, high cycle fatigue is generally described as failure associated with the load cycles being within the materials elastic limit and with failure typically taking place beyond 10000 cycles.

Beck and Stevens (1979) showed that decreasing the range of the load cycles following crack initiation from a higher load range, resulted in slower crack growth and longer life than if the higher cycle load range was maintained. The opposite occurred when loads were increased after the initiation of a crack, resulting in shorter life (Mahendran 1990). This agrees with the theory of cracks extending through the plastic zone at the crack tip where a larger stress cycle in the midst of

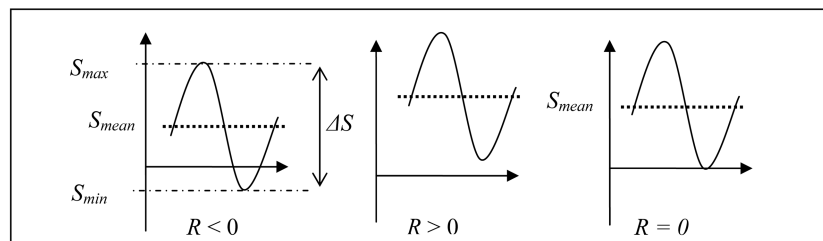


Fig. 7 Cyclic load - definitions

constant amplitude cycles, increases the plastic zone ahead of the crack tip (Smith 1991). As the crack grows through the plastic zone, its growth rate increases until the tip reaches a point where the zone size corresponds to that for the current stress amplitude at which time the crack grows at the constant amplitude rate. Smith (1991) notes that a large positive cycle ($R > 0$) can cause faster crack growth resulting from a bigger plastic zone than a large positive-negative cycle ($R < 0$).

Mahendran (1990) and Xu (1995) observed a range of crack propagation modes from extensive constant amplitude repeated load tests cycling at different load levels on the corrugated profile. The extensive data set tabulated by Mahendran (1990) was plotted and analysed to determine the effect of varying R on the fatigue performance, as shown in the S_{\max} - N curve of Fig. 8. This data shows the decreasing number of cycles to failure for the increasing load per cycle. The increasing R for a given S_{\max} (i.e. reducing ΔS), results in an increase in the number of cycles to failure. Henderson and Ginger (2005) show that the majority of wind load cycles have $R > 0$, suggesting that the majority of cyclic tests (e.g. L-H-L) with $R = 0$ may be conservative as they may not represent actual wind load acting on a roof.

Miner's rule is often used to predict the performance of metal components subjected to repeated loading. It was developed from research into the fatigue life of thick steel elements, such as machinery components subjected to a large number of low amplitude cycles (i.e. at stresses well below yield). Miner's rule (Eq. (3)) states that the amount of accumulated damage at a given level of stress is proportional to the number of cycles at that stress, n_i , to the total number for failure, N_i . That is, when the total equals one, failure will occur. Thus, fatigue failure may occur from a very large number of low level stress cycles or from a few cycles at a level near the ultimate static capacity.

$$n_1/N_1 + n_2/N_2 + n_3/N_3 + \dots = \sum_i(n_i/N_i) = 1 \quad (3)$$

For corrugated cladding, the different modes of crack initiation and propagation indicate a different fatigue response depending on the load level. Miner's rule relies on constant material properties and does not satisfactorily deal with this situation of changing profile shape, strength and stiffness (Beck and Stevens 1979, Mahendran 1993, Xu 1993). A modified Miner's rule was suggested that used different empirical constants depending on the load level. However, this method

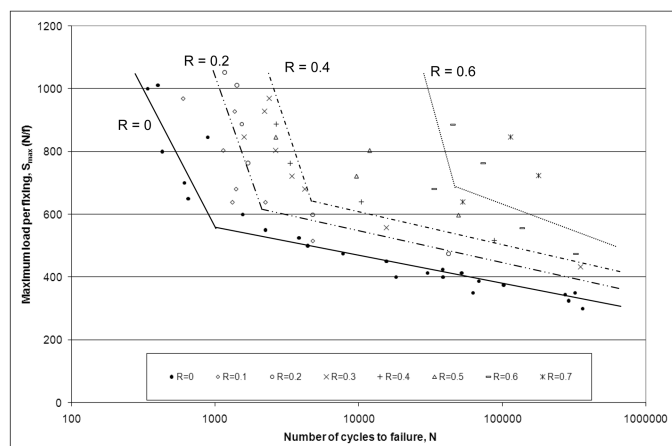


Fig. 8 S-N curve for corrugated cladding fastened without cyclone washers

did not adequately predict fatigue damage for cladding from cycle histories, especially when lower load cycles followed higher load level cycles. For complex loading histories with varying R values, a simple modified version of Miner's rule, described in Madayag (1969), is given in Eq. (4), where DI is the damage index, and K is an empirically derived parameter for when failure occurs. Xu (1995) suggests a value of 0.25 for K based on some cyclic tests on corrugated cladding. Xu notes however that extensive random fatigue loading tests are required to satisfactorily establish the value of K . Holmes (2002) used a closed form solution to derive cumulative damage and fatigue life in a similar manner, for along wind turbulence-induced (high-cycle) fatigue damage of slender structures.

$$DI = \sum_i (n_i/N_i) < K \quad (4)$$

The use of this modified version of Miner's rule presented here is not given for the accurate prediction of failure of a roofing system, but may be used for the quantitative comparison of the "damage" caused by the varying peaks and ranges of a fluctuating loading history.

5.3. Cycles in the wind

Wind loads on roof components have wide-band characteristics with a broad range of frequencies, as described by Ginger (2001). It is not obvious what constitutes a load cycle or how cycles should be counted. Of the many load cycle counting methods suggested, the "rainflow method" is generally regarded as the most realistic for predicting fatigue damage. In this method the cycles are presented in terms of means and ranges of the loads, from which the maximum, minimum and R values can be derived. The rainflow method, described by Amzalag, *et al.* (1994) and by Xu (1993) is used to determine the equivalent number of cycles over the observation time in this study.

In the pursuit of a realistic and practical low cycle fatigue test, Mahendran (1995), Xu (1995), and Kumar and Stathopoulos (1998) have used external pressure data from both model and full scale to determine load cycle counts using the rainflow counting method.

The matrix of cycle counts of external and net pressures obtained from the rainflow method for area A , for building orientations I and II are given in Tables 1 and 2 respectively. Each cell gives the number of cycles obtained. The Range and Mean, both in kPa, describe the range (ΔP) and mean (P_{mean}) that brackets the cycles in each cell. Approximately 68,400 and 72,700 cycles were obtained for the Net pressure cases for orientations I and II with 93% and 87% of these pressure cycles within the low 10% band of the peak pressure. Jancauskas, *et al.* (1994) obtained a matrix containing 75,000 cycles, with approximately 90% of their cycles within the 10% band.

The numbers of cycles applied in a L-H-L test, for a pressure of -4.8 kPa, derived in Section 3.2, are shown with brackets in Table 1(a). The L-H-L missed several large range cycles, however, the L-H-L method contained more than 10,000 cycles in the middle range when compared with the "design" cyclone for building orientation I. With regard to the net pressure cycles, the AS/NZS1170.2:2002 (Standards Australia 2002) calculated internal pressure (1.86 kPa) was added to give a design net pressure of -6.64 kPa. Although its peak value is similar to that derived from the net wind tunnel data, the L-H-L cycles greatly outnumbered the mid to high range wind tunnel load cycles as shown in Table 1b.

In calculating the damage index (DI), as defined by Eq. (4), S-N values for varying R values were extracted from the test data in Fig. 8. The rainflow matrix for building orientation I had a DI of 0.18 and 0.25 for the external and net cases while orientation II had 0.08 and 0.24. The two net

Table 1 Numbers of cycles for external and net pressures (kPa) for building orientation I

		(a) External									
Range		0.7	1.4	2.1	2.8	3.5	4.2	4.9	5.6	6.3	7.0
		0.0	0.7	1.4	2.8	2.1	3.5	4.2	4.9	5.6	6.3
Mean											
-0.7	0.0	27932	424								
-1.4	-0.7	20472	1196	231	39 (9000)						
-2.1	-1.4	10819	982	293	109	52 (1200)	8 (120)				
-2.8	-2.1	3814	423	136	66	44	20	7 (1)	1		
-3.5	-2.8	1072	140	38	11	8	1	5	7	2	
-4.2	-3.5	260	32	12	3	1					
-4.9	-4.2	32	4	1							
-5.6	-4.9	6	1								
-6.3	-5.6	2									
-7.0	-6.3										
Total		64409	3202	711	228	104	30	12	8	2	0
		(b) Net									
Range		0.7	1.4	2.1	2.8	3.5	4.2	4.9	5.6	6.3	7.0
		0.0	0.7	1.4	2.8	2.1	3.5	4.2	4.9	5.6	6.3
Mean											
-0.7	0.0	19432	154								
-1.4	-0.7	23918	1355	207	17						
-2.1	-1.4	13025	1124	361	137	45 (9000)	5 (1200)				
-2.8	-2.1	5180	588	181	76	66	32	15	5 (120)		
-3.5	-2.8	1546	204	48	18	8	3	6	2	7	3 (1)
-4.2	-3.5	422	69	22	3	3	1				
-4.9	-4.2	115	16	4	2						
-5.6	-4.9	7	3	1							
-6.3	-5.6	5									
-7.0	-6.3	2									
Total		63652	3513	823	254	122	41	21	7	7	3

cases had a similar DI even though the peak pressure for orientation I was nearly 2 kPa greater. However, orientation II contained a higher percentage of net cycles in the mid-pressure range increasing its DI to match that of orientation I, as reflected in the broader shape of Fig. 6(b) when

Table 2 Numbers of cycles for external and net pressures (kPa) for building orientation II

		(a) External									
Range		0.6	1.1	1.7	2.2	2.8	3.3	3.9	4.4	5.0	5.5
		0.0	0.6	1.1	1.7	2.2	2.8	3.3	3.9	4.4	5.0
Mean											
-0.6	0.0	25130	696								
-1.1	-0.6	29783	3560	679	124						
-1.7	-1.1	10196	1353	357	174	125	33				
-2.2	-1.7	2075	221	50	18	5	16	13	5		
-2.8	-2.2	415	43	16	5	1	2			2	
-3.3	-2.8	66	8								
-3.9	-3.3	7	2								
-4.4	-3.9										
-5.0	-4.4										
-5.5	-5.0										
	Total	67672	5883	1102	321	131	51	13	5	2	0
		(b) Net									
Range		0.6	1.1	1.7	2.2	2.8	3.3	3.9	4.4	5.0	5.5
		0.0	0.6	1.1	1.7	2.2	2.8	3.3	3.9	4.4	5.0
Mean											
-0.6	0.0	10477	245								
-1.1	-0.6	22319	2102	285	24						
-1.7	-1.1	19715	2698	937	331	87	9				
-2.2	-1.7	7795	1174	432	211	168	96	52	5		
-2.8	-2.2	2174	358	109	46	13	10	9	19	5	3
-3.3	-2.8	525	75	24	9	4					
-3.9	-3.3	117	25	2	1	1	1				
-4.4	-3.9	16	2								
-5.0	-4.4										
-5.5	-5.0										
	Total	63138	6679	1789	622	273	116	61	24	5	3

compared with Fig. 6(a). The rainflow method aggregates load cycles, thus ignoring sequence of loads and therefore the DI does not account for the effect of a high range cycles either preceding or following low cycles.

5.4. Application of fluctuating wind load

Advanced real time pressure loading systems capable of high flow have been developed for the “Three Little Pigs” (3LP) full scale house testing facility at the University of Western Ontario

(Kopp, *et al.* 2008). The pressure load actuators permit the application of actual temporally varying wind pressures to a representative test section of the building envelope. In collaboration with UWO, the CTS is using a PLA unit to further study the wind induced failures of cladding systems. The unit has been recently commissioned using a 2.0 x 0.8 m test chamber to accommodate a double 900 mm span length of cladding. Fig. 9 shows the air box with an inverted JR3 load cell to monitor the reaction at a centre support fastener and the PLA unit in the background.

The derived pressure trace for the 4.75 hour duration “design cyclone” for building orientation I (Fig. 6a) was applied to a cladding specimen installed in the air box test chamber. A one second portion of the requested pressure magnitude and the PLA achieved pressure trace is shown in Fig. 10, highlighting the resolution of the pressure fluctuations to less than 0.1 of a second.

Slight plastic deformation of the crests under the fixings was observed at approximately 80 minutes into the trace, shown in Fig. 6(a). Creasing (i.e., permanent deformation) of the crests adjacent to the fixings, occurred approximately 95 minutes into the trace. Initial cracking was observed at the creases, six minutes later. Crack growth increased, with cracks reaching lengths in the order of 20 mm, as shown in Fig. 11. However, there was no observed crack growth during the last quarter (~70 minutes) of the trace, during which the pressure progressively dropped.

The cladding “survived” the 4.75 hour “design” cyclone with its peak of 6.8 kPa, even though



Fig. 9 Air box with double 900 mm span cladding installed

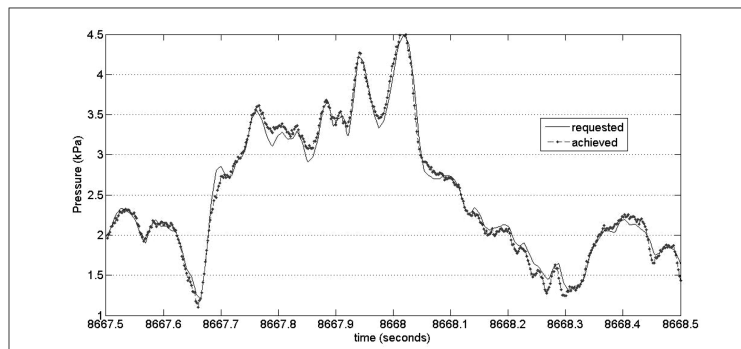


Fig. 10 Plot of PLA achieved response against target real time pressure trace

there was considerable cracking and deformation. The cladding resisted the applied loads by not disengaging from its supporting structure, which is defined as a successful outcome according to Australian cladding test standards.

The maximum allowable ULS design pressure for 0.42 mm corrugated cladding over continuous 900 mm spans, from a leading manufacturer’s design tables, is 4.75 kPa, which is based on the test method TR440. TR440 (Experimental Building Station 1978; revised in Standards Australia 1992) is a low cycle to high cycle test, and was the common test criteria for roofing prior to the recent introduction of L-H-L. In developing the original L-H-L test, Mahendran (1993) noted that the TR440 method was unconservative in comparison due to the ‘high’ load being located at the end of the test as opposed to the middle.

Fig. 12(a) shows a cladding specimen that was subjected to a L-H-L test in the CTS large air box, and was not able to resist a test load similar to that of a successful TR440 test (4.8 kPa). The magnitude of load level and low *R* promoted excessive yielding of the cladding under the screw head producing cracks at the screw hole which led to a quicker failure. The crack patterns were similar to that shown in Fig. 1(b), where the reaction at the screw was large due to the excessive screw spacing.

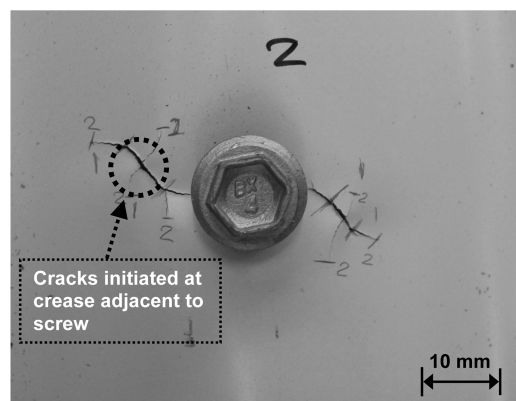


Fig. 11 Cracking of cladding at screw fixing

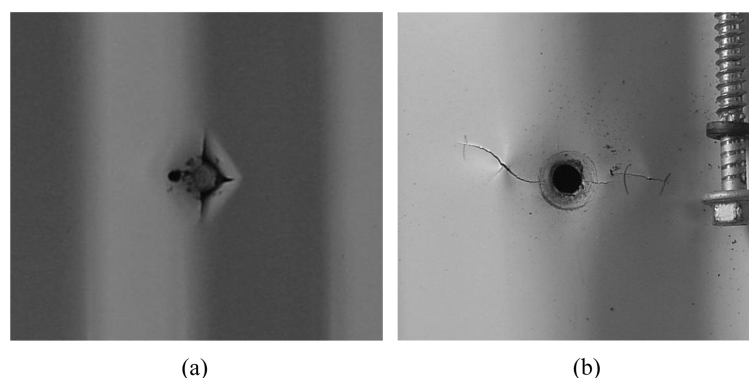


Fig. 12 Cracking patterns following L-H-L tests of cladding that (a) failed and (b) passed but had a 15% reduction in load per cycle

A second specimen was able to pass a L-H-L test with a 15% reduction of the load with crack patterns, as seen in Fig. 12(b), similar to that shown in Fig. 11, that is, with the early cycles not causing excessive yielding under the screw, creasing occurred away from the screw promoting crack growth at these stress concentrations which resulted in a longer crack path postponing failure. Cracks from the TR440 test were slight and radiated from the screw holes. The simulated wind trace has a vast majority of cycles $R > 0$, whereas, the L-H-L test has all cycles with $R = 0$, leading to a conservative outcome for this tested case.

The results showed that wind loads on roof cladding and its response leading to low cycle fatigue cracking was significantly influenced by the peak load, load range and the sequence of loading as also detailed by Mahendran (1993) and Xu (1995). When compared against the “design” pressure trace, the L-H-L test sequence produced a similar crack pattern. The L-H-L test is by necessity a simplification of the actual loading of the cladding and fixings during the passage of a cyclone, as it is conducted by different testing laboratories on different test equipment.

6. Conclusions

Fluctuating wind loads acting on the windward edge of the roof, representative of that on a cladding fastener on two orientations of a low-pitch low-rise building, were evaluated during the passage of a 4.75 hour “design” cyclone as defined by Jancauskas, *et al.* (1994). The fluctuating pressures were generated from wind tunnel data for a building in the NIST low-rise building database. Building orientation I resulted in peak suction pressures which were underestimated by AS/NZS1170.2:2002 (Standards Australia 2002), and approximately 2 kPa more than orientation II.

The rainflow method was used to obtain an estimate of loading cycles contained in the pressure traces for the building orientations. The pressure traces contained a few large cycles through to tens of thousands of small amplitude cycles, the majority with load ratios (R) greater than zero. The rainflow counts highlighted the larger magnitude of mid range cycles for building orientation II even though its peak was less than orientation I.

The rainflow cycle counts along with the S-N data with varying R were used to derive a damage index (DI) of the cladding for the different building orientations. The DI provides a means of quantifying the fatigue potential contained in a complex loading history. The estimated DI of each orientation was similar showing the importance of cycle numbers and that the highest peak pressure may not give the “worst” case for fatigue damage.

A real time pressure loading system (PLA) was used to apply the 4.75 hour simulated cyclonic wind pressure trace. Although sustaining plastic deformation and extensive cracking, the cladding sample resisted the applied loads, which were in excess of the cladding’s design span capacity.

The “design” cyclone, with increasing, then decreasing, wind speeds and direction changes generated increasing then decreasing pressures on the roof edge, in a manner similar to that specified in the Australian fatigue loading criteria, the Low High Low (L-H-L) test. A L-H-L test was able to complete the load cycles for a reduced pressure of 4.1 kPa with a similar degree of cracking for the simulated cyclone with a peak pressure of 6.8 kPa. The cracking patterns produced by the simulated wind loads were similar to fatigue cracks observed during cyclone damage surveys.

For a given peak pressure, the L-H-L was conservative when compared with the generated 4.75 hour pressure traces as it over estimated the number of mid range cycles and each L-H-L cycle started at zero load (i.e. $R = 0$), contributing to greater damage within fewer cycles for the tested

corrugated cladding. Load cycles starting and ending at a zero load are a limitation of typical laboratory cladding testing equipment.

Acknowledgements

This research was conducted at James Cook University. D.J. Henderson and J.D. Ginger gratefully acknowledge the support of an Australian Research Council Linkage Grant and Stramit Building Products as the industry partner. M.J. Morrison gratefully acknowledges scholarship support from the Natural Science and Engineering Research Council of Canada. G.A. Kopp gratefully acknowledges the support provided by the Canada Research Chairs Program.

References

- Amzallag, C., Gerey, J.P., Robert, J.L. and Bahuaud, J. (1994), "Standardization of the Rainflow Counting Method for Fatigue Analysis", *Int. J. Fatigue*, **16**, 287-293.
- Australian Building Codes Board (2007), *BCA 2007: Building Code of Australia*, Australian Building Codes Board, Canberra ACT, Australia.
- Beck, V.R. and Stevens, L.K. (1979), "Wind loading failures of corrugated roof cladding", *Institution of Engineers Australia Civil Engineering Transactions*, **CE21**(1), 45-56
- Darwin Reconstruction Commission (1976), *Darwin Area Building Manual*, Darwin, Australia.
- Experimental Building Station (1978), *Technical Record 440: Guidelines for the testing and evaluation of products for cyclone prone areas*, Sydney, Australia.
- Ginger, J.D. (2001), "Characteristics of wind loads on roof cladding and fixings", *Wind Struct.*, **4**(1), 73-84.
- Ginger, J.D. and Henderson, D.J. (2003), "Wind loads on roof cladding and fixings", *10th Australian Wind Engineering Workshop*, Sydney.
- Ginger, J.D., Henderson, D.J., Leitch, C. and Boughton, G.N. (2007), "Tropical Cyclone Larry: Estimation of wind field and assessment of building damage", *Aust. J. Struct. Eng.*, **7**, 209-224.
- Ginger, J.D., Holmes, J.D. and Kopp, G.A. (2008), "Effect of building volume and opening size on fluctuating internal pressure", *Wind Struct.*, **11**(5), 361-376.
- Harper, B.A., Kepert, J.D. and Ginger, J.D. (2008), "Guidelines for converting between various wind averaging periods in tropical cyclone conditions", Report submitted to World Meteorological Organization.
- Henderson, D.J. and Ginger, J.D. (2005), "Fatigue failure of roof components subjected to wind loading", *Australian Structural Engineering Conf.*, Newcastle.
- Henderson, D.J., Ginger, J.D. and Reardon, G.F. (2001), "Performance of light gauge metal roof cladding subjected to cyclonic wind loading – A review", *Australasian Wind Engineering Society Workshop*, Townsville.
- Ho, T.C.E., Surry, D., Morrish, D. and Kopp, G.A. (2005), "The UWO contribution to the NIST aerodynamic database for wind loads on low buildings: Part 1. Archiving format and basic aerodynamic data", *J. Wind Eng. Ind. Aerod.*, **93**, 1-30.
- Holmes, J.D. (2002), "Fatigue under along-wind loading—closed-form solutions", *Eng. Struct.*, **24**, 109–114.
- Jancauskas, E.D., Mahendran, M. and Walker, G.R. (1994), "Computer simulation of the fatigue behaviour of roof cladding during the passage of a tropical cyclone", *J. Wind Eng. Ind. Aerod.*, **51**, 215-227.
- Kopp, G.A., Morrison, M.J., Iizumi, E., Henderson, D. and Hong, H.P. (2008), "The 'Three Little Pigs' Project: Hurricane Risk Mitigation by Integrated Wind Tunnel and Full-Scale Laboratory Tests", submitted to *ASCE Nat. Hazards* (September, 2008).
- Kumar, K.S. and Stathopoulos, T. (1998), "Fatigue analysis of roof cladding under simulated wind loading", *J. Wind Eng. Ind. Aerod.*, **77-8**, 171-183.
- Madayag, A. (1969), *Metal Fatigue: Theory and design*, Wiley & Sons, New York.
- Mahendran, M. (1990), "Fatigue behaviour of corrugated roofing under cyclic wind loading", *Civil Engineering Transactions*, I. E. Aust.
- Mahendran, M. (1993), "Simulation of Cyclonic Wind Forces on Roof Claddings by Random Block Load

- Testing”, Cyclone Testing Station Technical Report No. 38, James Cook University.
- Mahendran, M. (1995), “Towards an Appropriate Fatigue Loading Sequence for Roof Claddings in Cyclone Prone Areas”, *Eng. Struct.*, **17**, 476-484.
- Morgan, J. and Beck, V. (1977), “Failure of sheet metal roofing under repeated wind loading”, *Civil Engineering Transactions*, I. E. Aust.
- Oh, J.H., Kopp, G.A. and Incelet, D.R. (2007), “The UWO contribution to the NIST aerodynamic database for wind loads on low buildings: Part 3. Internal pressures”, *J. Wind Eng. Ind. Aerod.*, **95**, 755-779.
- Smith, R.N.L. (1991), *Basic fracture mechanics*, Oxford, Butterworth-Heinemann.
- St. Pierre, L.M., Kopp, G.A., Surry, D. and Ho, T.C.E. (2005), “The UWO contribution to the NIST aerodynamic database for wind loads on low buildings: Part 2. Comparison of data with wind load provisions”, *J. Wind Eng. Ind. Aerod.*, **93**, 31-59.
- Standards Australia (1992), *Methods of testing sheet roof and wall cladding - Resistance to wind pressures for cyclone regions*, AS-4040.3:1992, Standards Australia, Sydney NSW, Australia.
- Standards Australia (2002), *Structural design actions – Part 2: Wind actions*, AS/NZS-1170.2:2002, Standards Australia, Sydney NSW, Australia.
- Walker, G.R. (1975), *Report on Cyclone Tracy – Effect on buildings – Dec 1974*, Australian Dept of Housing and Construction.
- Xu, Y.L. (1993), “Wind Induced Fatigue Loading on Roof Cladding of Low-Rise Buildings”, Cyclone Testing Station Technical Report, Townsville, James Cook University.
- Xu, Y.L. (1995), “Fatigue Performance of Screw-Fastened Light-Gauge-Steel Roofing Sheets”, *J. Struct. Eng.* ASCE, **121**, 389-398.